Linearized AVO inversion with supercritical angles

Jon Downton (Veritas DGC) and Charles Ursenbach (CREWES, University of Calgary), Calgary

2005 CSEG National Convention

Summary
Contrary to popular belief, a linearized approximation of the Zoeppritz equations may be used to accurately estimate the reflection coefficient for angles of incidence up to and beyond the critical angle. These supercritical reflection coefficients are complex implying a phase variation with offset in addition to the amplitude variation with offset. This linearized approximation is used as the basis for a new AVO waveform inversion capable of truly incorporating wide angle information.

Introduction
Supercritical reflection coefficients arise in situations of interest to explorationists. In trying to determine density through AVO large angles of incidence and offset are used in the inversion (Downton, 2005). It is required by most AVO inversion approaches using a linearized approximation that only incidence angles less than the critical angle are used. Since the reliability of the estimates is proportional to the range of angles used in the inversion this limits the reliability of the resulting density estimates.

In addition the critical angle also plays an important role for heavy oil plays in north eastern Alberta. The Paleozoic often goes critical due to the large velocity contrast between the overlying clastics and underlying carbonates. This becomes a problem because the large supercritical reflection coefficients obscure the overlying zone of interest. The traditional way of dealing with this is to limit the range of angles used in the AVO inversion. This is problematic since the critical angle may be as low as 25 degrees, again limiting reliability of the estimates of the AVO inversion.

Limiting the angles used in the AVO inversion is due to the common and mistaken believe that the Aki and Richards (1980) linearized approximation (equation 5.44) of the Zoeppritz equation is only valid for subcritical angles of incidence. For example Nicolao et al. (1993) state that the linearized approximation is only valid for precritical angles. In fact, Aki and Richards (1980) state as a precondition for using the linearized approximation (equation 5.44) that the angles of incidence and transmission must be less than 90 degrees, thus precluding the critical angle.

This seems to be supported if the Aki and Richards (1980) equation for the PP reflection coefficient *R(p)* is written in terms of horizontal slowness *p*

$$R(p) = \frac{1}{2}\left(1 - 4\beta^2 p^2\right)\frac{\Delta\rho}{\rho} + \frac{1}{2\sqrt{1-\alpha^2 p^2}}\frac{\Delta\alpha}{\alpha} - 4\beta^2 p^2 \frac{\Delta\beta}{\beta}, \qquad (1)$$

where ρ, α, and β are the average density, P-wave and S-wave velocities, and the differentials $\Delta\rho$, $\Delta\alpha$, and $\Delta\beta$ are the change in layer properties for the density and velocity. As written, the reflection coefficient calculated by equation (1) must be real for homogenous waves (i.e. *p* is real). However, supercritical reflection coefficients are complex, making use of the complex numbers to contain the phase information.

If however, equation (1) is parameterized in terms of the average angle of incidence θ

$$R(\theta) = \frac{1}{2}\left(1 - 4\frac{\beta^2}{\alpha^2}\sin^2\theta\right)\frac{\Delta\rho}{\rho} + \frac{1}{2\cos^2\theta}\frac{\Delta\alpha}{\alpha} - 4\frac{\beta^2}{\alpha^2}\sin^2\theta\frac{\Delta\beta}{\beta}, \qquad (2)$$

the reflection coefficient can become complex. This is a consequence of the fact that θ is the average of incidence and transmitted angles, $(\theta_r + \theta_t) / 2$. The incidence angle, θ_r, is always real, but the transmitted angle becomes complex for angles beyond the critical angle:

$$\theta_t = \frac{\pi}{2} - i\cosh^{-1}\left(\frac{\alpha_2}{\alpha_1}\sin\theta_r\right), \qquad \frac{\alpha_2}{\alpha_1}\sin\theta_r \geq 1. \qquad (3)$$

To illustrate this, a simple convolutional model was generated using both the Zoeppritz equation and equation (2) to generate the reflection coefficients. The density, P-wave and S-wave velocity layer information used to construct this model are based on a well log from north eastern British Columbia drilled for the Halfway (Downton, 2005). The synthetic is shown with a 10/14-90/110 Hz trapezoidal zero phase filter. Both synthetics are shown without moveout, geometrical spreading or other losses, highlighting differences that arise solely due to the linearized approximation. The synthetic data generated using equation (2) (Figure 1a) closely approximates that using the Zoeppritz equation (Figure 1b) as evidenced by the difference display of the two (Figure 1c). Figures 2a, 2b and 2c show amplitude extractions taken from the two models at time samples corresponding to interfaces which include supercritical angles. The synthetic model generated using equation (2) closely matches the results generated using the Zoeppritz equation.

Linearized Inversion

The above discussion suggests two issues that must be dealt with if supercritical angles are to be included in the AVO inversion. It is evident that the phase changes as a function of angle of incidence. This is problematic for traditional AVO inversion schemes which work on a sample by sample basis. These AVO inversions ignore the wavelet and so can not handle these phase changes. This suggests some sort of AVO waveform inversion (Buland and Omre, 2003; Simmons and Backus, 1986; Downton and Lines, 2004) should be used.

Secondly, the amplitudes of the synthetic data are very large at the far offsets compared to the near offsets. Real seismic data does not look like this due to geometrical spreading, attenuation, and other losses. To address this, the seismic data is normally preconditioned to correct for these losses prior to the AVO inversion. However, including angles close to critical make these corrections unstable. Figure 3 shows the geometrical spreading losses calculated following Cervany (2001). Note the large change in scalars close to the critical angle. If the inverse of this is applied as a geometrical correction this will introduce high frequency noise into the seismic data. It is much more stable to apply this as a forward operation prior to the application of the wavelet. This once again is easily done as part of an AVO waveform inversion.

The approach of Downton and Lines (2004) is easily modified to incorporate both these considerations. The basis of the inversion is Downton and Lines (2004) equation (1)

$$\begin{bmatrix} \mathbf{d}_1 \\ \vdots \\ \mathbf{d}_N \end{bmatrix} = \begin{bmatrix} \mathbf{W}\mathbf{N}_1\mathbf{F}_1 & \mathbf{W}\mathbf{N}_1\mathbf{G}_1 & \mathbf{W}\mathbf{N}_1\mathbf{H}_1 \\ \vdots & \vdots & \vdots \\ \mathbf{W}\mathbf{N}_N\mathbf{F}_N & \mathbf{W}\mathbf{N}_N\mathbf{G}_N & \mathbf{W}\mathbf{N}_N\mathbf{H}_N \end{bmatrix} \begin{bmatrix} \mathbf{r}_P \\ \mathbf{r}_S \\ \mathbf{r}_d \end{bmatrix}, \tag{4}$$

where $\mathbf{r}_p$,$\mathbf{r}_s$,$\mathbf{r}_d$ are the P- and S-wave velocity, and density reflectivity respectively. These are all vectors whose elements correspond to different time samples. Likewise the elements of the data vector $\mathbf{d}_n$ represent the processed seismic data for the n^{th} offset for the corresponding time samples. The block matrices describe the physics of the problem. The matrices **F, G**, and **H** are diagonal matrices that contain weights that describe how the amplitude changes as a function of offset. These weights are complex and follow from equation (2). Following Claerbout (1992), the block matrix $\mathbf{N}_n$ performs NMO. This operator can be constructed using whatever offset traveltime relationship one desires. In order to invert data at large angles of incidence, it is important to correctly position the event without introducing residual NMO. In this case, a higher order correction is used following Castle (1994). This has the advantage of introducing high-order terms without introducing the theoretical complications of intrinsic anisotropy. Implicit in this derivation is that the velocity is known *a priori* and that static corrections are applied. Lastly, **W** is a convolution matrix which contains the source wavelet. In order to insure the output of this operation is real, the convolution is implemented in the frequency domain where Hermitian symmetry is imposed. Gain corrections such as geometrical spreading may be implemented appropriately scaling each of the diagonal matrices **F, G**, and **H**.

Applying these three operators in series, the block matrices $\mathbf{F}_n$,$\mathbf{G}_n$,$\mathbf{H}_n$ model the offset dependent reflectivity from the zero offset reflectivity, $\mathbf{N}_n$ applies NMO and **W** convolves the offset dependent reflectivity with the source wavelet modeling the band limited seismic data with NMO. The inversion of equation (4) can be thought of as three separate inversion problems, deconvolution, inverse NMO and AVO inversion. Downton and Lines (2004) solve this using conjugate gradient and high-resolution constraints. Equation (4) is solved in a similar fashion.

Inversion Results

The synthetic model shown in Figure (1) was rerun with moveout, geometrical spreading and other losses. The result (Figure 4a) was used as the input into the AVO waveform inversion. Figure 4b shows the estimated data from the AVO inversion while Figure 4c shows the difference between the estimated and actual data. The AVO inversion was able to estimate the original data quite accurately. Figure 5 shows a comparison between the estimated and reference zero offset reflectivity. Again the inversion was able to estimate the reflectivity quite accurately.

Discussion and Conclusions

This inversion approach is much more theoretically accurate and better conditioned than traditional AVO inversion performed on a time sample-by-sample basis on a limited angle range. The method is approaching the accuracy of reflectivity modeling (Kennett,1984) where only compressional waves and first order reflectivity terms are considered. Because the problem is linearized, and only band limited reflectivity are being solved for, the algorithm is much faster than reflectivity inversion (Sen and Stoffa, 1995). By linearizing the problem we have introduced the additional constraint that the fractional changes in layer parameters must be small, but this is typically a good assumption as based on well log data.

Acknowledgements

The lead author would like to thank Veritas for permitting him to publish this and Dave Gray for many conversations that helped to lead to this research. In addition we would like to thank Jan Dewar for many helpful suggestions in proofreading.

References

Aki, K., and Richards P.G., 1980, Quantitative seismology: theory and methods: W.H. Freeman and Co.

Buland, A., and Omre, H., 2003, Bayesian linearized AVO inversion: Geophysics, 68, 185-198.

Castle, R.J., 1994, Theory of normal moveout: Geophysics, 59, 983-999.

Červeny, V., 2001, Seismic ray theory: Cambridge University Press.

Claerbout, J.F., 1992, Earth Soundings Analysis: Processing versus Inversion: Blackwell Scientific Publications.

Downton, J.E., 2005, Seismic parameter estimation from AVO inversion: Ph.D. Thesis, University of Calgary.

Downton, J., and Lines, L., 2004, Three-term AVO waveform inversion: 74th Ann. Internat. Mtg.: Soc. of Expl. Geophys.

Kennett, B.L.N., 1984, Seismic wave propagation in stratified media: Cambridge University Press.

de Nicolao, A., Drufuca, G. and Rocca, F., 1993, Eigenvectors and eigenvalues of linearized elastic inversion: Geophysics, 58, 670-679.

Sen, M., and Stoffa P.L., 1995, Global optimization methods in geophysical inversion: Elsevier Science Publishers.
Simmons, J.L., Jr. and Backus, M.M., 1996, Waveform-based AVO inversion and AVO prediction error: Geophysics, 61, 1575-1588.

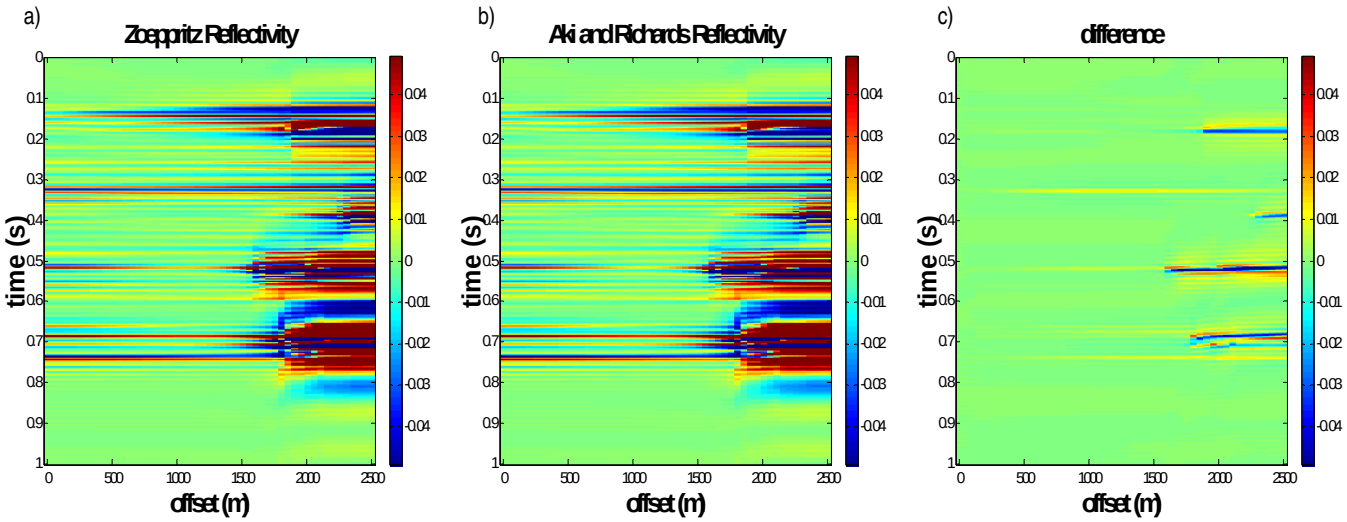

Figure 1: Synthetic model (a) generated with Zoeppritz equation, (b) generated with equation 2 and (c) difference between (a) and (b).

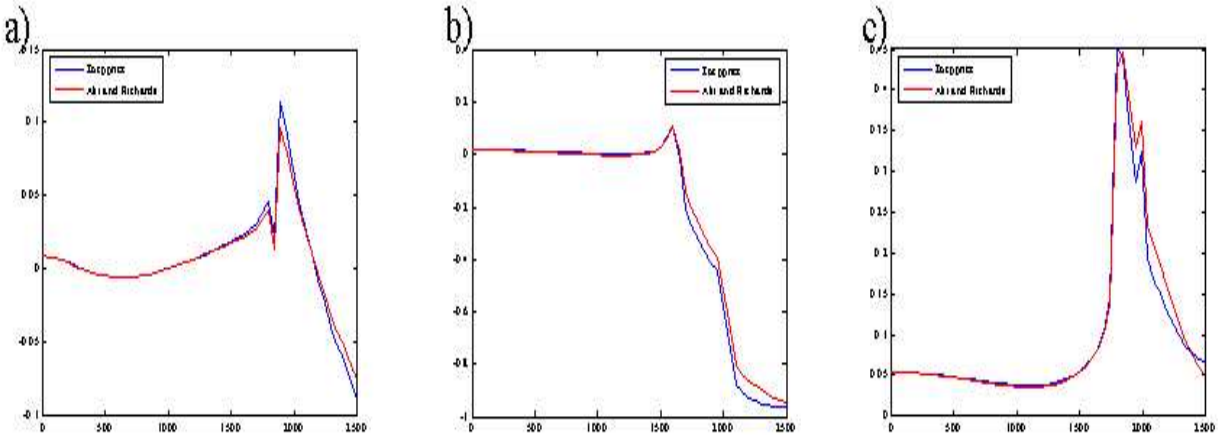

Figure 2: Comparison of extracted amplitude at selected times from Figure 1a and Figure 1b. Figure 2a) is at 172 ms, 2b) at 520 ms, and c) at 684 ms. The x-axis is offset in meters.

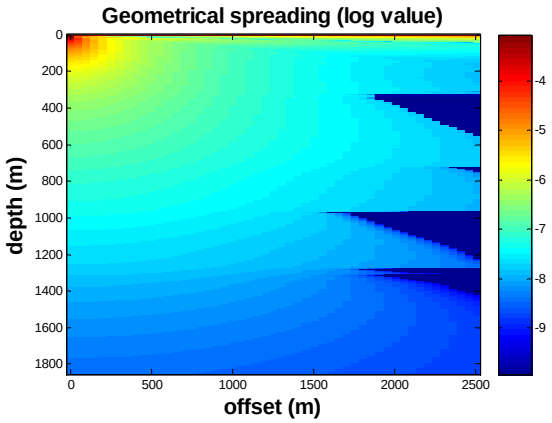

Figure 3: Geometrical spreading losses shown with a log scale. The critical angle generates a poorly illuminated zone shown in dark blue.

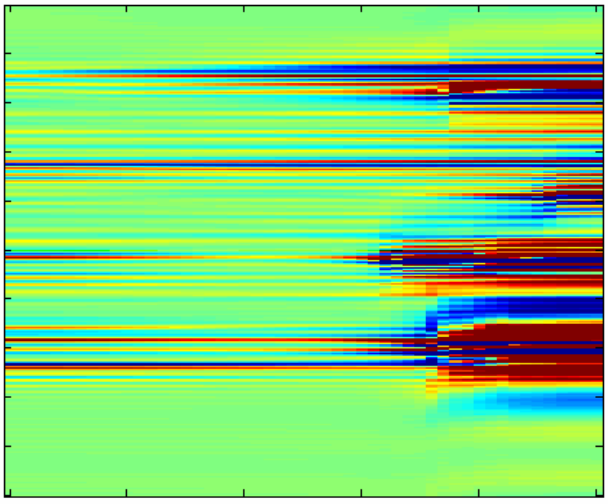

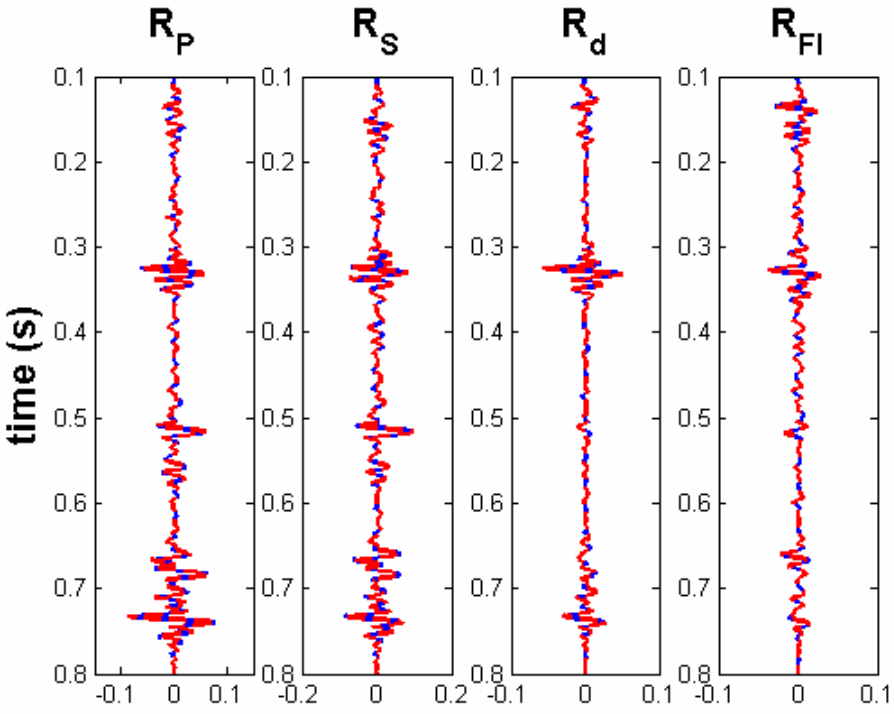
R_P
R_S
R_d
R_Fl
time (s)
0.1
0.2
0.3
0.4
0.5
0.6
0.7
0.8
-0.1
0
0.1
-0.2
0.2